gia, S. Smith, *Science* **265**, 1599 (1994). Their analytic approximation for the elasticity is given by $Fp/k_BT = 0.25*(1 - x/L)^{-2} - 0.25 + x/L$, where $F$ is the force applied across the ends, $p$ is the persistence length, and $k_BT$ is the thermal energy.
21. D. E. Smith, T. T. Perkins, S. Chu, *Macromolecules* **29**, 1372 (1996).
22. R. G. Larson, T. T. Perkins, D. E. Smith, S. Chu, *Phys. Rev. E* **55**, 1794 (1997).
23. Following the example of W. D. Volkmuth and R. H. Austin [*Nature* **358**, 600 (1992)], we made our flow cells by etching silicon wafers with KOH and anionically bonding Pyrex coverslips to the silicon to seal the top surface of the channels. Vertical side walls along the inlet and outlet channels were achieved by rotating the pattern by 45° to the crystal axis [C. Hu and S. Kim, *Appl. Phys. Lett.* **29**, 582 (1976)]. To generate the flow, we used a syringe pump (Isco model 100 D) which was temperature-stabilized at 22.7°C. A ~100:1 fluid shunt bypassing the flow cell was used to operate the pump at flow rates >40 μl/min. The velocity field was calibrated by tracking fluorescent beads near the stagnation point and showed $v_y = \dot{\varepsilon}\, y$, confirming that a uniform elongational flow had been achieved. Our imaging and digitization system was the same as previously described (*17*), except we used a water immersion objective (Zeiss 40× C-APO NA 1.2) and stroboscopically illuminated the DNA to eliminate the blurring of the image due to camera lag. Our measurements of the equilibrium coil size generally did not yield $2\,R_G$ but something slightly larger due to blooming in the camera. Once the chain is extended about two times the equilibrium size, the blooming is reduced and the measurements correspond closely to the actual extension. We stained the λ-DNA (New England Biolabs) with YOYO-1 (Molecular Probes) at a dye:base-pair ratio of 1:4 for >1 hour. The experiment was performed in a high viscosity ($\eta$ = 41 centipoise) buffer consisting of 10 mM tris-HCl, 2 mM EDTA, 10 mM NaCl, 4% β-mercaptoethanol, ~50 μg/ml glucose oxidase (Boehringer Mannheim), ~10 μg/ml catalase (Boehringer Mannheim), ~18% (w/w) glucose and ~40% (w/w) sucrose. The viscosity of each solution was measured in a temperature-stabilized viscometer and adjusted as needed. The flow cell was mounted on a copper block and stabilized to 22.7° ± 0.2°C.
24. To prevent any predeformation of the polymer before entering the elongational flow, we used a cross-slot flow cell with channels 650 μm wide and 220 μm deep and imaged the polymers at the center of depth of the channel ($z_{center}$ = 110 μm) where the applied shear ($\dot{\gamma} \equiv \partial v_x/\partial z$) was negligible. Because of the mismatch in the index of refraction of the immersion fluid (water) and the high viscosity buffer, we determined $z_{center}$ by measuring the velocity of fluorescent beads in the inlet as a function of depth and fitting this velocity to a parabolic, Poiseuille velocity field. Because of their finite size ($R_G \cong 0.7$ μm), polymers at $z_{center}$ still experienced some shear. For our highest strain rate ($\dot{\varepsilon} = 0.86\ s^{-1}$), the corresponding reduced shear rate in the inlet was $\dot{\gamma}\tau_{relax} = 0.5$, which is below the expected onset of deformations (*2*). We observed no deformation of the polymers in the inlet at $\dot{\varepsilon} = 0.86\ s^{-1}$, but a doubling of the flow rate led to modest (~4 μm) predeformation of some molecules. We used 25-mm-long inlet channels, which allowed any molecule deformed upon entering the flow cell sufficient time (>8 $\tau_{relax}$) to relax back to equilibrium before entering the elongational flow.
25. At the lower strain rates, there were not distinct, well preserved conformations, but the large variation $t_{onset}$ still occurred. The polymers had the general appearance of a dumbbell configuration subject to a large fluctuations in extension and shape.
26. We determined $\tau_{relax}$ = 3.89 s by averaging the relaxation of 14 individual, highly extended molecules. The relaxation time we report is from a fit over the region where $x/L < 0.3$ to $\langle x(t)x(t)\rangle = c \exp(-t/\tau_{relax}) - 2\,R_G$, where $\tau_{relax}$, $c$, and $R_G$ were free parameters. This is directly related to the relaxation of the stress in the fluid via $\sigma_E = n\,\langle x \cdot F(x)\rangle$, because in the limit of small deformation, $F(x)$ is linear in $x$ and this yields $\sigma_E(t) \sim \langle x(t)x(t)\rangle$. Thus, our characterization of $\tau_{relax}$ via stress relaxation is made in the region ($x/L < 0.3$) where $\tau_{relax} \cong \tau_1$ because the contribution of higher order relaxation modes should be negligible (*2*). When scaled to $\eta$ = 1 centipoise and for the change in length caused by staining, our $\tau_{relax}$ for unstained, λ-DNA in water is 0.061 s (*8*). This analysis does not take into account any possible changes in persistence length. No change in solvent quality was measured between sucrose and glycerol viscosity-enhanced aqueous buffered solution used for the measurements of $\tau_{relax}$ and $\tau_1$, respectively (*35*). Our $\tau_{relax}$ reported here is different than relaxation time determined from $\langle x(t)\rangle = c \exp(t/\tau) - R_G$, which yields $\tau$ = 6.2 s, and is the relaxation time we reported in an earlier experiment where the DNA was tethered to a bead (*35*).
27. The longer DNA molecules were concatemers of λ-DNA (up to 250 μm). We were unable to systematically investigate the dynamics of longer molecules, because we did not have an adequately monodisperse sample and could not independently measure the length of individual molecules.
28. The results presented here should not be generalized to polymers in a mixed elongational and shearing flow or to polymers in an elongational flow that were presheared. Our data indicates that the processes involved in the diverse dynamics arise from the variation in $t_{onset}$ and from internal configurations (that is, folds). In mixed flows, a large fraction of the molecules are partially extended because of shearing, and this effect may eliminate some of the internal constraints that led to the observed dynamics.
29. S. Daoudi and F. Brochard, *Macromolecules* **11**, 751 (1978); P. G. de Gennes, *Scaling Concepts in Polymer Physics* (Cornell Univ. Press, Ithaca, NY, 1979); E. J. Hinch, *Phys. Fluids* **20**, 522 (1977).
30. J. M. Rallison, *J. Non-Newtonian Fluid Mech.* **68**, 61 (1997). For simulations of longer chains, see P. S. Doyle, E. S. G. Shaqfeh, and A. P. Gast [*J. Fluid Mech.* **334**, 251 (1997)].
31. G. Ryskin, *Phys. Rev. Lett.* **59**, 2059 (1987); *J. Fluid Mech.* **178**, 423 (1987); R. G. Larson, *Rheol. Acta* **29**, 371 (1990); D. H. King and D. F. James, *J. Chem. Phys.* **78**, 4749 (1983).
32. A. Peterlin, *Makromol. Chem.* **44**, 338 (1961).
33. R. Keunings, *J. Non-Newtonian Fluid Mech.* **68**, 85 (1997).
34. B. H. Zimm, *J. Chem. Phys.* **24**, 269 (1956); P. E. Rouse, *ibid.* **21**, 1272 (1953).
35. T. T. Perkins, S. R. Quake, D. E. Smith, S. Chu, *Science* **264**, 822 (1994).
36. We thank G. Fuller, D. Hoagland, R. Larson, R. Pecora, and B. Zimm for helpful discussions and J. Shott for generous aid in lithographic design. Supported in part by grants from the U.S. Air Force Office of Scientific Research, NSF, and the Human Frontiers Foundation and by an endowment established by Theodore and Frances Geballe. We acknowledge the generous assistance of J. Spudich, including support through NIH grant GM33289 to J. Spudich. D.E.S. was supported by a fellowship from the Program in Mathematics and Molecular Biology at the University of California, Berkeley, through NSF grant DMS 9406348. S.C. was supported in part by a Guggenheim fellowship during the course of this work.

18 February 1997; accepted 8 May 1997

# Surface Stress in the Self-Assembly of Alkanethiols on Gold

Rüdiger Berger,* Emmanuel Delamarche, Hans Peter Lang, Christoph Gerber, James K. Gimzewski, Ernst Meyer, Hans-Joachim Güntherodt

Surface stress changes and kinetics were measured in situ during the self-assembly of alkanethiols on gold by means of a micromechanical sensor. Self-assembly caused compressive surface stress that closely followed Langmuir-type adsorption kinetics up to monolayer coverage. The surface stress at monolayer coverage increased linearly with the length of the alkyl chain of the molecule. These observations were interpreted in terms of differences in surface potential. This highly sensitive sensor technique has a broad range of applicability to specific chemical and biological interactions.

Molecular and biomolecular layers are scientifically appealing for a wide range of potential applications (*1*, *2*). Alkanethiols, which are known to self-organize into well-ordered, densely packed films, represent a model molecular system for controlling surface properties (*3*, *4*). These self-assembled monolayers (SAMs) are used in applications such as microcontact printing (*5*) and voltametric microsensors (*6*), and they have recently been applied to molecular host-guest recognition (*7*).

There is little information available on the mechanical properties of SAMs, particularly concerning the nature of surface stress in films during the formation process, because it is difficult to follow the structural evolution of monolayer self-assembly. One recent approach (*8*) used scanning tunneling microscopy to infer the growth kinetics of alkanethiol SAMs indirectly from snapshot images obtained at various coverages. Here, we used micromechanical sensors to gather quantitative data on surface stress changes that develop during the self-assembly process of HS-

R. Berger and H. P. Lang, IBM Research Division, Zürich Research Laboratory, CH-8803 Rüschlikon, Switzerland, and Institute of Physics, University of Basel, CH-4056 Basel, Switzerland.
E. Delamarche, Ch. Gerber, J. K. Gimzewski, IBM Research Division, Zürich Research Laboratory, CH-8803 Rüschlikon, Switzerland.
E. Meyer and H.-J. Güntherodt, Institute of Physics, University of Basel, CH-4056 Basel, Switzerland.
*To whom correspondence should be addressed.

$(CH_2)_{n-1}$-$CH_3$ for $n$ = 4, 6, 8, 12, and 14, where $n$ is the number of carbon atoms in the alkyl chain (Fig. 1A). Micromechanical sensors are attracting increasing interest in science and technology for in situ process control (*9–11*) because they feature high sensitivity, small size, and compatibility with Si microelectronic fabrication (*12*).

V-shaped micromechanical silicon nitride ($SiN_x$) cantilevers with a 20-nm gold receptor layer evaporated on one side were used as sensors for gas-phase adsorption of alkanethiols (Fig. 1B). Scanning force microscopy techniques (*13*) were used to detect sensor deflections down to the picometer scale. A laser beam reflected off the cantilever's apex onto a quadrant photodiode used as a position-sensitive detector (PSD) indicated sensor displacement. Alkanethiol vapors were generated by placing a few microliters of alkanethiol in the center of a glass beaker, which was then closed by a shutter. After thermal equilibrium was reached, the shutter was opened, thereby exposing the sensor to alkanethiol vapor (*14*).

The sensor deflection, derived from the PSD voltage, was measured as a function of time for experiments with alkanethiols of various chain lengths (Fig. 2A). In all cases, we observed a strong response in deflection, which saturated at a permanent value (between ~50 and 200 nm) corresponding to the expansion of the receptor side of the sensor (Fig. 1D). This saturation developed on a time scale similar to that previously reported for monolayer formation by chemisorption on gold (*15*). In contrast, reference experiments performed with octane vapor showed no comparable response.

Several transduction mechanisms can contribute to these observations. Thermal effects are known to produce bendings as a consequence of the bimetallic effect (*10*). Self-assembly of alkanethiols on gold is exothermic, with an enthalpy of adsorption $\Delta E \approx -150$ kJ mol$^{-1}$ (*16*). Hence, chemisorption of a monolayer of alkanethiols on the sensor's receptor surface (~$10^{10}$ molecules) can produce ~25 nJ of heat. The sensor's calculated transient bending caused by the reaction heat has the observed sign of deflection but is on the order of only 0.5 nm (*10*); thereafter, thermal effects are negligible. Nor can the gravimetric deflection resulting from the molecular loading (calculated to be ~5 pm) account for the observed bending. On the basis of both the permanent nature of the deflection and its magnitude, we attribute the response to surface stress (*17–19*). Stoney's formula (*20*) relates the sensor curvature radius $R$ to the surface stress $\sigma$ acting on the sensor,

$$\sigma = \frac{Et_s^2}{6R(1-\nu)} \quad (1)$$

where $R^{-1} = 3\Delta z/2L^2$, $L$ is length, $E$ is Young's modulus, $\nu$ is Poisson's ratio of the sensor material, $\Delta z$ is deflection, and $t_s$ is sensor thickness.

The alkyl chains in the monolayer exhibit a tilting away from the surface normal to reduce chain-to-chain separation and to optimize the chains' attractive intermolecular van der Waals interaction. We intuitively expected to observe a tensile surface stress, corresponding to a bending toward the SAM, from

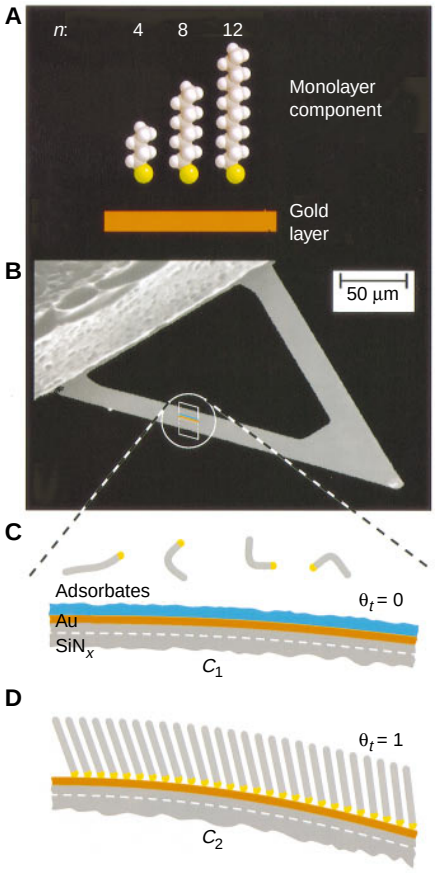


**Fig. 1.** (**A**) Alkanethiols assemble spontaneously from solution or vapor onto gold. The specific monolayer component is drawn in a space-filling model for butanethiol ($n$ = 4), octanethiol ($n$ = 8), and dodecanethiol ($n$ = 12). (**B**) Scanning electron micrograph of the Au-coated $SiN_x$ cantilever showing the sensor's receptor surface. (**C**) The sketch shows a cut perpendicular to the surface through the sensor layers as used for the self-assembly process. Coverage of chemisorbed alkanethiols on the sensor $\theta_t$ = 0: The sensor is covered by adsorbates in air (average thickness ~1 nm), which causes a bending, $C_1$, of the sensor. (**D**) $\theta_t$ = 1: When the sensor is exposed to alkanethiol vapor, a SAM is formed. This causes a bending, $C_2$, which compresses the underlying substrate.

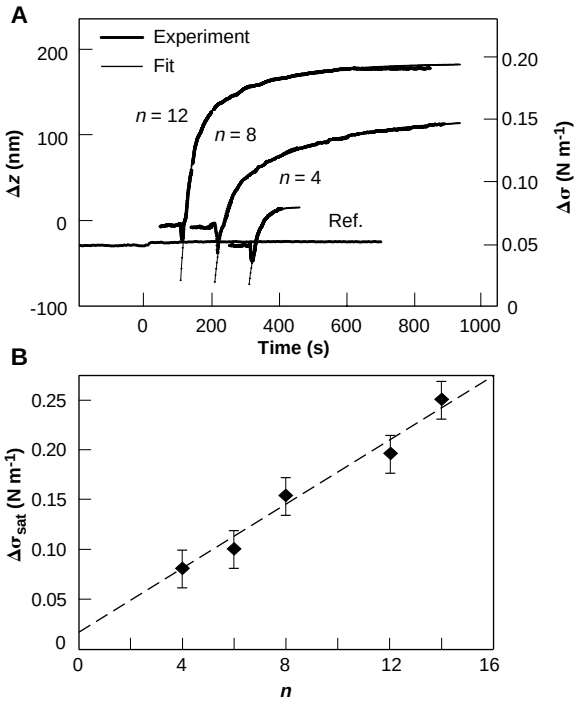


**Fig. 2.** (**A**) Deflection, $\Delta z$, and changes in surface stress, $\Delta\sigma$, of the sensors are plotted as a function of time for exposure to alkanethiol and a reference vapor. Reference experiments consisted of exposing the sensor to vapors of alkanes—molecules that do not chemisorb on gold—and showing the background noise. The reference curve used octane and is representative of all controls. In the reference experiment, no deflection was observed, except for a small signal attributed to the removal of the shutter. In contrast, the sensors started bending immediately after exposure to alkanethiol vapors. We estimate the exposure of the sensor to butanethiol molecules to be ~1.5 × $10^{20}$ molecules cm$^{-1}$ s$^{-1}$ under our experimental conditions. A faster response for lighter alkanethiols, corresponding to their higher vapor pressures, was observed. Each alkanethiol curve was fitted by a LM adsorption isotherm, which determines the zero point of the stressograms. In our experiments with butanethiol and octanethiol, LM fits the entire stress curve. For dodecanethiol, we found a deviation from the LM beginning above ~80% coverage, indicating a decrease of the sticking coefficient. From our data, we calculate the average tension $\sigma_t = \sigma_{sat}t_f^{-1}$ in a monolayer of thickness $t_f$ to be 0.16 ± 0.03 GPa for all five SAMs studied. Before exposure, the sensor response was recorded in air for ~1 min, which reflected the initial amount of adsorbates of the gold layer from our laboratory environment. Initial values of deflection before exposure do not influence the LM fitting procedure. (**B**) The change in surface stress at saturation coverage obtained for $n$ = 4, 6, 8, 12, and 14 is plotted as a function of alkyl chain length. The value of $\Delta\sigma_{sat}$ at $n$ = 0 reflects the constant surface stress contribution from sulfur chemisorption, the formation of depressions in the gold, or both.

this effect. Surprisingly, all the chemisorbed alkanethiols we investigated caused compressive surface stress during self-assembly. Except for the initial few seconds of exposure, a Langmuir adsorption isotherm model (LM), for which $\theta \propto 1 - \exp(-\kappa t)$, where $\theta$ is the coverage, $t$ is the time, and $\kappa$ is the reaction rate, fits the stress curves (*21*). LM describes the coverage dependence of alkanethiol adsorption both in solution (*22*) and from the vapor phase (*15*). Because the stress curves follow LM characteristics, we can conclude that the surface stress is proportional to the number of molecules adsorbed.

The saturated surface stress $\sigma_{sat}$ generated by SAMs of alkanethiols increased linearly with chain length (Fig. 2B). From these data, we conclude that the compressive surface stress change is directly proportional to alkyl chain length. The molecular weight of linear alkanethiols is the principal determinant of the degree of structural order of SAMs on gold (*4*). In particular, short-chain monolayers of butanethiol have pronounced disorder and have been described as liquid-like films at room temperature (*23*). In contrast, SAMs with longer chains such as dodecanethiol form monolayers with a high degree of order. Consequently, our observations indicate that $\Delta\sigma$ is insensitive to structural parameters.

In terms of electrostatic interactions, the apparent dipole moment of the SAM is considered to contain a contribution from the $Au^+$-$S^-$ head group and from the $S^-$-$alkyl^+$ chain. Even at low coverage, the sulfurs are bound to the gold, and the $-CH_3$ tail groups tend to emerge at the air-monolayer interface (*4*), providing an average apparent dipole moment. This apparent dipole moment increases linearly with $n$ (*24*), resulting in a linear increase of electrostatic repulsion. Such dipolar repulsive forces in adsorbate-adsorbant systems are generally expected to produce surface stresses on the order of $10^{-3}$ N m$^{-1}$ (*25*), which is consistent with the magnitude of our measurements. In particular, the linear relations between $\Delta\sigma$ and both $\theta$ and $n$ are consistent with an electrostatic model.

Upon careful inspection, the stressograms display small, monotonic, step-like variations observable at higher magnification (Fig. 3). These variations are clearly above the noise level given by the reference experiment. The steps are typical for all stress curves performed with $n \geq 8$, and we tentatively associate them directly with the self-assembly process. They may result from local changes of concentration in the immediate environment of the sensor (for instance, as a result of turbulence), which can lead to inhomogeneous chemisorption rates. In general, inhomogeneities in the self-assembly process can be detected in situ and in real time with a surface stress resolution of $10^{-7}$ N m$^{-1}$ by means of standard-size sensors. This corresponds to a change of zepto ($10^{-21}$) molar quantities in our experiments on SAMs.

The kinetics of SAM formation display clearly resolved minima at the beginning of each chemisorption process. X-ray photoelectron spectroscopy and second-harmonic generation studies of self-assembly of alkanethiols in solutions have led to the proposal that the initial phase of the reaction includes the replacement of residual adsorbates on the gold surface by chemisorbed alkanethiols (*26*). This process was confirmed for our samples by means of ellipsometry (*27*). All surface stress curves except the reference curve in Fig. 2A reveal the replacement process as a release of $11 \times 10^{-3}$ to $19 \times 10^{-3}$ N m$^{-1}$ of residual surface stress (*28*) during the first ~10 s of exposure to alkanethiols (Fig. 1C).

This replacement of one molecular layer by another can be extended to the specific binding of a molecule to a receptor layer. To demonstrate this concept, we used SAMs of $\omega$-functionalized alkanethiols as acceptors for molecular recognition. We studied the influence of gas-phase hexylamine on mercaptohexadecanoic acid SAMs (Fig. 4). A clear decrease in $\Delta\sigma$ was observed when hexylamine molecules "docked" onto the SAMs' carboxylic end groups. These observations are in qualitative agreement with a preliminary report of nonspecific binding of albumin on SAMs (*29*).

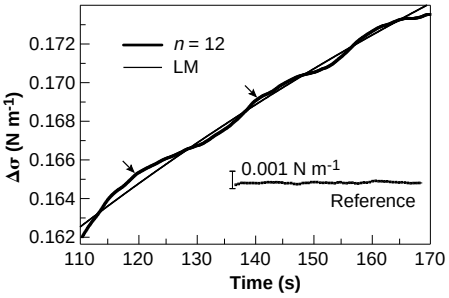


**Fig. 3.** The stressogram for dodecanethiol self-assembly at higher magnification displays step-like variations of surface stress. The reference, plotted for comparison, displays the background noise. The small variation, indicated by the arrows, is caused by an attomolar quantity of molecules.

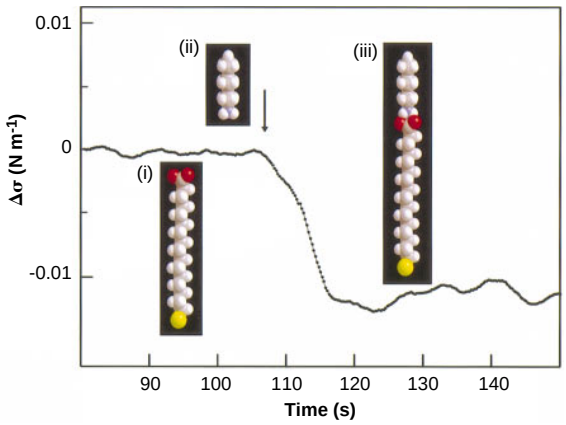


**Fig. 4.** Model experiment of a sensor coated with mercaptohexadecanoic acid SAM (i) as a functionalized surface. Mercaptohexadecanoic acid acts as a specific receptor to bind hexylamine (ii) as an acceptor molecule. The resulting salt bridge formation (iii) is detected by a change in surface stress, which was normalized to that of the mercaptohexadecanoic monolayer. The arrow indicates the beginning of the exposure of the sensor to hexylamine vapors.

## REFERENCES AND NOTES


1. G. M. Whitesides, J. P. Mathias, C. T. Seto, *Science* **254**, 1312 (1991).
2. H. Dugas, *Bioorganic Chemistry, A Chemical Approach to Enzyme Action* (Springer, New York, 1996).
3. R. G. Nuzzo and D. L. Allara, *J. Am. Chem. Soc.* **105**, 4481 (1983).
4. C. D. Bain *et al*., *ibid.* **111**, 321 (1989).
5. A. Kumar, H. A. Biebuyck, G. M. Whitesides, *Langmuir* **10**, 1498 (1994).
6. J. J. Hickman, D. Ofer, P. E. Laibinis, G. M. Whitesides, M. S. Wrighton, *Science* **252**, 688 (1991).
7. K. D. Schierbaum *et al*., *ibid.* **265**, 1413 (1994).
8. G. E. Poirier and E. D. Pylant, *ibid.* **272**, 1145 (1996).
9. J. W. Gardner, *Microsensors* (Wiley, New York, 1994).
10. J. K. Gimzewski, Ch. Gerber, E. Meyer, R. R. Schlittler, *Chem. Phys. Lett.* **217**, 589 (1994).
11. J. R. Barnes, R. J. Stephenson, M. E. Welland, Ch. Gerber, J. K. Gimzewski, *Nature* **372**, 79 (1994).
12. S. C. Minne, S. R. Manalis, A. Atalar, C. F. Quate, *Appl. Phys. Lett.* **68**, 1427 (1996).
13. G. Binnig, C. F. Quate, Ch. Gerber, *Phys. Rev. Lett.* **56**, 930 (1986).
14. We used commercially available sensors [length = 180 μm, width = 18 μm, thickness = 0.6 μm, $\nu$ = 0.23, and $E$ = 150 GPa (Park Scientific Instruments, Mountain View, CA)], from which we removed the gold layer. Ti (~0.5 nm) and Au (~20 nm) were evaporated just before each experiment. The measured normalized voltage difference $\Delta V$ of the PSD indicates the vertical deflection of the sensor. This displacement was calibrated in situ by standard force-distance curves determining $\Delta z$. We estimated the temperature of the micromechanical sensor to be 25°C [R. Berger, Ch. Gerber, J. K. Gimzewski, E. Meyer, H.-J. Güntherodt, *Appl. Phys. Lett.* **69**, 40 (1996)]. Solvents and reagents were used as received from the supplier or as otherwise indicated. Alkanethiols (FLUKA, 95%) were further purified with a short chromatography column to remove high-weight impurities and were then kept under vacuum (~5 mbar) for 4 hours to remove lower molecular residual thiols. A glass beaker with an opening of 2 cm was filled with 20 μl of the thiol solution, closed with a shutter, and placed 5 cm from the sensor under ambient conditions. Humidity and temperature were kept constant at 50 ± 3% and 22° ± 0.5°C during all experiments. The sensor head was shielded against vibrations, turbulence, and thermal drifts.
15. R. C. Thomas, L. Sun, R. M. Crooks, *Langmuir* **7**, 620 (1991).

16. R. G. Nuzzo, L. H. Dubois, D. L. Allara, *J. Am. Chem. Soc.* **112**, 558 (1990).
17. F. Liu and M. G. Lagally, *Phys. Rev. Lett.* **76**, 3156 (1996).
18. A. Grossmann, W. Erly, J. B. Hannon, H. Ibach, *ibid.* **77**, 127 (1996).
19. D. Sander, A. Enders, J. Kirschner, *Appl. Phys. Lett.* **67**, 1833 (1995).
20. G. G. Stoney, *Proc. R. Soc. London Ser. A* **82**, 172 (1909).
21. A. Ulman, *Ultrathin Organic Films* (Academic Press, London, 1991).
22. K. A. Peterlinz and R. Georgiadis, *Langmuir* **12**, 4731 (1996).
23. N. Camillone III, C. E. D. Chidsey, G. Liu, T. M. Putvinski, G. Scoles, *J. Chem. Phys.* **94**, 8493 (1991).
24. S. D. Evans and A. Ulman, *Chem. Phys. Lett.* **170**, 462 (1990).
25. H. Ibach, *J. Vac. Sci. Technol.* **A12**, 2240 (1994).
26. M. Buck, M. Grunze, F. Eisert, J. Fischer, F. Träger, *J. Vac. Sci. Technol.* **A10**, 926 (1992).
27. In addition to performing stressometry, we followed the self-assembly of alkanethiols in a similar setup by determining the thicknesses of forming SAMs with ellipsometry. These experiments confirmed the complete replacement of residual contaminants by alkanethiol molecules and also reflected the time scale of forming monolayers as detected by the micromechanical sensor. The measurements confirmed the theoretically expected thicknesses for all SAMs, indicating the high purity of the alkanethiol used. We used this technique to follow the contamination kinetics of physisorbed adsorbates of the clean gold surface. This process emerged on a time scale of ~2 hours under our typical laboratory conditions.
28. T. Thundat, R. J. Warmack, G. Y. Chen, D. P. Allison, *Appl. Phys. Lett.* **64**, 2894 (1994).
29. H. J. Butt, *J. Colloid Interface Sci.* **180**, 251 (1996).
30. We thank D. Anselmetti, H. Biebuyck, P. Guéret, and H. Rohrer for helpful discussions and support, and P. Vettiger and the IBM Zürich micromechanics group for their contributions to optimizing sensor performance. Partially supported by the Swiss National Science Foundation (NFP 36) and Swiss Priority Program MINAST 7.04.

6 March 1997; accepted 7 May 1997

# The Role of Antibody Concentration and Avidity in Antiviral Protection

M. F. Bachmann,* U. Kalinke, A. Althage, G. Freer,† C. Burkhart,‡ H.-P. Roost, M. Aguet, H. Hengartner, R. M. Zinkernagel§

Neutralizing antibodies are necessary and sufficient for protection against infection with vesicular stomatitis virus (VSV). The in vitro neutralization capacities and in vivo protective capacities of a panel of immunoglobulin G monoclonal antibodies to the glycoprotein of VSV were evaluated. In vitro, neutralizing activity correlated with avidity and with neutralization rate constant, a measure of on-rate. However, in vivo, protection was independent of immunoglobulin subclass, avidity, neutralization rate constant, and in vitro neutralizing activity; above a minimal avidity threshold, protection depended simply on a minimum serum concentration. These two biologically defined thresholds of antibody specificity offer hope for the development of adoptive therapy with neutralizing antibodies.

Antibody responses against chemically defined haptens, proteins, and pathogens have been well characterized, and the properties of polyclonal sera and monoclonal antibodies (mAbs) specific for these antigens have been studied in detail in vitro. Increased avidities and on-rates of antibodies have been postulated to provide increased in vivo effectiveness and protection (*1*). However, such a correlation has only rarely been analyzed for antibodies specific for, and protective against, infectious agents in vivo. Low-avidity ($10^5$ $M^{-1}$) opsonizing antibodies can protect against bacteria (*2*), and some studies have correlated in vitro virus neutralization titers with in vivo protection (*3*), whereas others have found no such relation (*4*). Avidity, on-rate, neutralizing activity, or antibody concentration have not previously been analyzed with respect to protective activity in vivo. We used a panel of mAbs (*5*–*7*) and polyclonal antibodies derived from high-titer secondary and hyperimmune responses to test whether characteristics of antibodies in vitro can predict protective efficiency in vivo—that is, whether increased avidity of immunoglobulin G (IgG) provides protection at lower serum concentrations.

VSV is a rhabdovirus closely related to rabies virus. It is highly neurotropic and may cause neurological disease and death in mice. Recovery of mice from primary infections or resistance against reinfection depends on neutralizing IgG antibody responses; $CD8^+$ T cells are not involved, whereas mice lacking B cells always die (*8*, *9*). The surface envelope of VSV contains ~1200 identical glycoprotein molecules that form a regular and densely ordered pattern of spike tips; these tips are the only sites accessible to neutralizing antibodies (*10*). Neutralization of rhabdoviruses is mediated by the prevention of docking of the virus to cellular receptors. This requires a minimum of 200 to 500 IgG molecules bound per virion (*11*). The Fc portions of antibodies are not crucial for antiviral protection in vivo or in vitro (*8*, *12*).

We previously described a set of virus-neutralizing mAbs derived from mice immunized with VSV serotype Indiana (VSV-IND) (*6*, *7*). Virtually all of a collection of 62 mAbs that neutralize VSV bind to a single antigenic site on VSV-G comprising three overlapping subsites with avidities ranging from $2 \times 10^7$ $M^{-1}$ to $9 \times 10^9$ $M^{-1}$

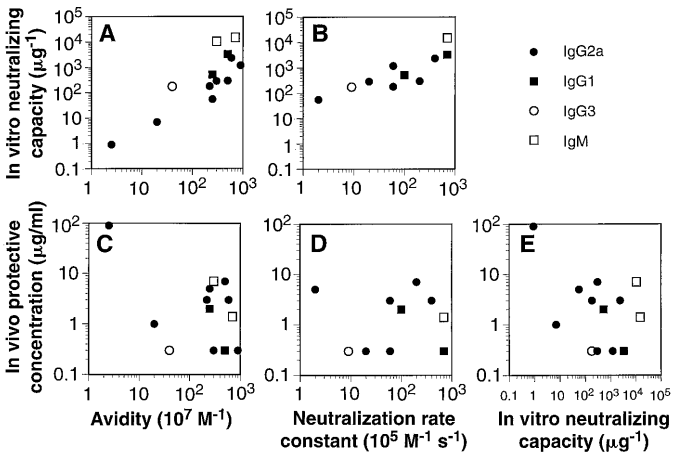


**Fig. 1.** Correlation of in vitro and in vivo parameters of mAbs. (**A** and **B**) Avidity (A) and neutralization rate constant (B) of mAbs, correlated with their in vitro neutralizing capacity. (**C** to **E**) Avidity (C), neutralization rate constant (D), and in vitro neutralizing capacity (E) of the same mAbs did not correlate with their in vivo protective concentration (see Table 1). Linear regression revealed correlation coefficients *r* of 0.86 (A), 0.93 (B), and <0.4 [(C) to (E)].

M. F. Bachmann, U. Kalinke, A. Althage, G. Freer, C. Burkhart, H.-P. Roost, H. Hengartner, R. M. Zinkernagel, Institute of Experimental Immunology, Department of Pathology, University Hospital Zürich, Schmelzbergstrasse 12, CH-8091 Zürich, Switzerland.
M. Aguet, Swiss Cancer Institute, Chemin Des Boveresses 155, 1066 Epalinges, Switzerland.

*Present address: Department for Medical Biophysics, Ontario Cancer Institute, Toronto, Ontario M5G 2M9, Canada.
†Present address: Department of Biomedicine, University of Pisa, I-S6127 Pisa, Italy.
‡Present address: Department of Pathology and Microbiology, University of Bristol, Bristol BS8 1TD, UK.
§To whom correspondence should be addressed. E-mail: RZI@pty.smtp.usz.ch